Research Square

Preprints are preliminary reports that have not undergone peer review.
They should not be considered conclusive, used to inform clinical practice,
or referenced by the media as validated information.

Structure-function design of 3D-printable whole lotus root-Schizophyllum commune composite gels for dysphagia foods with reduced starch digestibility

Xuanzi Liu
Wuhan Polytechnic University
Xuanxuan Cao
Wuhan Polytechnic University
Jinfeng Wang
Wuhan Polytechnic University
Huanhuan Liu
Wuhan Polytechnic University
Hao Dong
Wuhan Polytechnic University
Yang Yi
Wuhan Polytechnic University
Xueyu Jiang
jiangxy@whpu.edu.cn

Wuhan Polytechnic University

Article

Keywords: 3D food printing, Dysphagia food, Schizophyllum commune, Structure-function relationship, In vitro starch digestion

Posted Date: August 28th, 2026

DOI: https://doi.org/10.21203/rs.3.rs-10506550/v1

License: This work is licensed under a Creative Commons Attribution 4.0 International License.
Read Full License

Additional Declarations: No competing interests reported.

Abstract

Designing foods for older adults with coexisting dysphagia and impaired glycemic control requires simultaneous control of bolus texture, printability, and starch digestibility. Here, whole lotus root powder (WL) was combined with *Schizophyllum commune* powder (SC; 0–32%, w/w relative to WL) to construct 3D-printable composite gels. Rheology, printing stability, texture, water mobility, molecular interactions, microstructure, *in vitro* starch digestion, and International Dysphagia Diet Standardization Initiative (IDDSI) tests were integrated to establish composition-structure-function relationships. SC reduced the storage and loss moduli, indicating partial disruption of the continuous starch network, but increased post-shear recovery from 13.1% to 28.2%. At SC contents of at least 24%, particle filling, water immobilization, and interfacial interactions increased hardness and resistance to deformation. FTIR, LF-NMR, CLSM, and microscopy collectively showed that SC altered hydrogen-bonding, redistributed water, inhibited short-range starch ordering, and produced a more densely packed composite skeleton despite reduced continuity of the starch-rich phase. These changes decreased glucose release and reduced 180-min starch hydrolysis from 13.03% to 9.33% (28.4%). The estimated glycemic index decreased from 65.60 to 52.76 at 32% SC, while all formulations met the qualitative IDDSI Level 5 criteria evaluated in this study. Thus, SC enabled a tunable balance among extrusion, structural recovery, oral texture, and starch digestibility, providing a structure-guided strategy for developing 3D-printed dysphagia-oriented foods. Clinical swallowing safety and postprandial glycemic responses require further validation.

1. Introduction

Population ageing, is increasing the prevalence of dysphagia, a condition that compromises safe and efficient oral intake and can reduce dietary quality. Dysphagia commonly coexists with chronic metabolic disorders, including diabetes, creating a practical need for foods that are easy to process orally while limiting rapid postprandial glucose release (Wang, Jiang, et al., 2025). Most texture-modified foods are designed primarily for swallowing, whereas their carbohydrate digestibility and glycemic potential receive less attention.

WL is a promising matrix for texture-modified foods because it retains starch, dietary fiber, polysaccharides, polyphenols, and endogenous proteins and can be processed into printable pastes (Wang, Peng, et al., 2025).Its starch-rich composition supports gelatinization and shape formation, although the resulting products may release glucose rapidly. Improving the nutritional functionality of WL without sacrificing extrusion and post-deposition stability therefore requires a complementary structuring ingredient. SC is an edible mushroom rich in polysaccharides, dietary fibers, and fungal proteins (Nuinamwong et al., 2024). Fungal polysaccharides and can increase matrix viscosity, modify starch gelatinization and retrogradation, restrict enzyme accessibility, and reduce starch digestion (Wunjuntuk et al., 2021). However, whole SC powder is a multicomponent ingredient, and its concentration-dependent effects on starch-network continuity, water mobility, interfacial interactions, printing behavior, and oral texture remain unclear.

Extrusion-based 3D food printing provides a route to personalize food geometry and portion size for individuals with dysphagia. Successful printing, however, requires a narrow rheological window in which the ink exhibits shear-thinning during extrusion, rapidly recovers after deposition, and retains sufficient strength to support successive layers (Liu et al., 2024). Studies focused solely on printability do not fully explain how molecular interactions and multiscale structures jointly govern texture and digestibility. Establishing this structure–function relationship is particularly important when a particulate, fiber-rich mushroom powder is incorporated into a starch-based gel.

This study therefore investigated WL-SC composite gels containing 0–32% SC (w/w relative to WL). We hypothesized that SC would disrupt the long-range starch network while, above a concentration threshold, densifying the composite skeleton through hydration, particle filling, and non-covalent interactions. Rheology, collapse and drop resistance, texture, static stability, LF-NMR, FTIR, molecular-interaction analysis, CLSM, optical microscopy, SEM, *in vitro* starch digestion, and IDDSI tests were combined to determine how SC concentration controls printability, swallowing-oriented texture, and estimated glycemic potential. The novelty lies in resolving the apparent trade-off between starch-network weakening and particle-driven structural reinforcement and linking this multiscale mechanism to both printing performance and starch digestibility.

2. Materials and methods

2.1. Materials

Fresh lotus roots (Elian No.5) were supplied by Wuhan Jinshui Qiliang Agricultural and Sideline Products Co., Ltd. (Wuhan, China). *Schizophyllum commune* was provided by Hubei Minxin Ecological Agriculture Technology Co., Ltd. (Shiyan, China). All reagents were of analytical or commercial grade, as appropriate. Deionized water was produced using an ECO-Q15YT purification system (HHItrch Instrument Co., Ltd., Shanghai, China).

2.2. Sample preparation

Fresh lotus roots were washed, peeled, and cut into 3–4 mm thick slices. The slices were dried in a hot-air oven at 75 ℃ for 24 h, ground, and sieved through a 100-mesh sieve to obtain WL (Wang et al., 2026). WL (10 g) was dispersed in water (50 g), and SC was added at 0, 0.8, 1.6, 2.4 or 3.2 g, corresponding to 0, 8, 16, 24, or 32% (w/w, relative to WL). Each suspension was homogenized at 10,000 rpm for 1 min and gelatinized in a water bath at 90 ℃ for 15 min. The formulations were designated WL, SC-8%, SC-16%, SC-24%, and SC-32%, respectively, and are collectively referred to as SC-WLG.

2.3. Rheology test

Rheological measurements were performed using a rheometer (NETZSCH Kinexus Lab+, Malvern, UK) equipped with a 40 mm diameter parallel plate geometry and a 1 mm gap. Samples were equilibrated at 25 ℃, and measurements were conducted in triplicate. The linear viscoelastic region (LVR) was identified by amplitude sweeps before dynamic testing. Frequency sweeps were conducted at 0.1%

strain (within the LVR) over an angular-frequencies rang of 0.1–100 rad/s to determine storage modulus (*G′*) and loss modulus (*G″*). Steady-shear viscosity was measured from 0.1 to 100 s^{-1}. Three-interval thixotropy test comprised 120 s at 0.1 s^{-1}, 120 s at 100 s^{-1}, and 120 s at 0.1 s^{-1}. Strain sweep measurements were carried out at 1 Hz frequency with oscillatory stress ranging from 0.1 to 1000% to examine deformation-dependent viscoelastic properties. Creep-recovery behavior was analyzed by applying a constant shear stress of 10 Pa for 120 s, followed by 420 s of recovery after stress removal.

2.4. Printing and collapse test

Gelatinized samples were printed using a 3D food printer (FOODBOT-D1, Changxing Shiyin Technology Co., Ltd., China) fitting with a 1.5 mm nozzle, and the printing speed was 15 mm/s. Post-deposition stability was assessed by allowing printed structures to collapse under their own weight and recording changes in morphology. The collapse deformation index expressed as the percentage change in diameter relative to the initial diameter.

2.5. Drop test

Impact resistance was evaluated by dropping each printed sample (WL, SC-8%, SC-16%, SC-24%, and SC-32%) once from a height of 50 cm onto a flat surface. Front and top views were recorded immediately after impact, and deformation, cracking, layer separation, and overall structural integrity were assessed.

2.6. Textural properties

Texture profile analysis (TPA) of the printed samples was performed at 25 ℃ using a texture analyzer (TMS-Pro, FTC, USA) equipped with a P/10 probe. The test speed was 60 mm/min, the compression ratio was 50%, and the trigger force was 0.05. N. Hardness, springiness, chewiness, breaking force, and fracturability were obtained from the force-deformation curves.

2.7. Static stability

The physical stability of the unprinted dispersions was evaluated at room temperature static observation after 0.5 and 1 h. The deposition rate (DR) was calculated using Eq. (1), where $H_{0.5h}$ and H_{1h} represented the heights of the deposited layer at 0.5 and 1 h, respectively. Lower DR values indicated reduced stratification and greater dispersion stability.

$$DR(\%) = H_{0.5\mathrm{h}} / H_{1h} \times 100 \quad (1)$$

2.8. Low-field nuclear magnetic resonance test (LF-NMR)

Water distribution and migration in SC-WLG were investigated using a LF-NMR analyzer (NMI20-040V, Suzhou New-mark Analytical Instrument Co., Ltd., China), equipped with an external circulating thermostat. Transverse relaxation times were measured using a Q-CPMG pulse sequence with 4 scan repetitions, 3000 echoes, a recycle delay of 13.8 s, and pulse intervals of 200 ms for both the 90° and 180° pulse. Relaxation peaks were assigned to water populations with different mobilities, and their relative areas were calculated.

2.9. Fourier transform infrared spectroscopy (FTIR)

Samples were ground with KBr at a 1:100 (w/w) ratio, pressed into pellets, and analyzed with a Frontier FT-IR spectrometer (PerkinElmer, UK). Spectra were collected from 4000 to -400 cm^{-1} for 32 scans at a resolution of 4 cm^{-1}. The O-H stretching region and the 1047/1022 cm^{-1} absorbance ratio were used to assess hydrogen-bonding and short-range starch order, respectively. Protein secondary structures were estimated by deconvolution and curve fitting of the amide I region (1600–1700 cm^{-1}).

2.10. Intermolecular force analysis

Intermolecular forces were evaluated with minor modifications to the method of Zheng (Zheng et al., 2021). Briefly, sample (0.25 g) was dispersed in 5 mL of the following solutions: (A) 0.05 mol/L NaCl, (B) 0.6 mol/L NaCl, (C) 0.6 mol/L NaCl + 1.5 mol/L urea, (D) 0.6 mol/L NaCl + 8 mol/L urea, (E) 0.6 mol/L NaCl + 8 mol/L urea + 0.5 mol/L β-mercaptoethanol. Mixtures were homogenized, incubated at 4 ℃ for 1 h, and centrifuged at 8000 rpm for 10 min. Protein content in the supernatant was quantified via the Bradford assay. Differences in protein solubility between B-A, C-B, D-C, and E-D were assigned to ionic bonds, hydrogen bonds, hydrophobic interactions, and disulfide bonds, respectively.

2.11. Confocal laser scanning microscopy (CLSM)

Sample was mix with freshly prepared 0.05% Nile Blue staining solution (for staining SC) and 0.02% Rhodamine B staining solution (for staining proteins) (Qiu et al., 2024). After incubation in the dark at 25 ℃ for 10 min, the samples were observed by CLSM using excitation wavelengths of 633 and 546nm. Two non-overlapping fields were randomly selected for each sample, and the experiment was performed in duplicate.

2.12. Optical microscopy (OM)

The morphology of the gelatinized starch phase was observed using an optical microscope (ICX41, China). A small amount of sample was spread on a glass slide, covered with a coverslip, and gently compressed to remove air bubbles. The magnification was set at 40× objective lens and 10× eyepiece.

2.13. Scanning electron microscopy (SEM)

The microstructure of gels was observed via SEM (SU8600, Hitachi, Japan). Samples were frozen at -80 ℃, fractured in liquid nitrogen, gold-sputtered for 90 s, and imaged at 500× and 1000× magnification with an accelerating voltage of 5 kV.

2.14. *In vitro* starch digestion

In vitro digestion was simulated according to the Englyst method with minor modifications (Zhou et al., 2026). Sample (0.2 g) was dispersed in 5 mL of sodium acetate buffer (0.2 M, pH 5.2) vortexed, and heated at 80 ℃ for 30 min. After cooling and equilibrating at 37 ℃ for 15 min, 5 mL of digestive enzyme mixture containing α-amylase (300 U/mL) and amyloglucosidase (60 U/mL) was added, together with two glass beads. The flasks were shaken continuously, and 1 mL aliquot were collected at 0, 20, 60, 120,

and 180 min. Enzyme reaction was terminated immediately by adding absolute ethanol (5 mL). After centrifugation at 5000 rpm for 15 min, glucose in the supernatant was quantified using a glucose assay kit.

2.15. International dysphagia diet standardization initiative (IDDSI) assessment

The swallowing-oriented texture of SC-WLG was assessed using qualitative IDDSI tests. For the fork-pressure test, a standard four-tined fork was pressed slowly onto 3D-printed lotus-shaped samples (approx. 20 mm side length), and deformation was recorded. For the fork-drip test, samples were lifted on a fork with approximately. 4 mm tine spacing to assess structural integrity retention between tines. For the spoon-tilt test, samples were placed on a smooth spoon and tilted laterally to evaluate fluidity and adhesiveness.

2.16. Statistical analysis

Data were expressed as mean ± standard deviation (SD) deviation from three independent replicates. Statistical analysis was performed using SPSS Statistics 21.0 (IBM, USA). Differences among formulations were evaluated by one-way analysis of variance followed by Duncan's multiple-range test, with $p < 0.05$ considered significant. Figures were prepared using Origin 2024.

3. Results and Discussion

3.1. Rheological properties

Rheological measurements were used to resolve the balance between extrusion under shear and structural support after deposition. During the amplitude sweep (Fig. 1a), *G′* exceeded *G″* within the LVR for all formulations, confirming predominantly elastic gel behavior. Both moduli declined as SC content increased, with SC 32% exhibiting the lowest modulus. The decline indicated that SC particles and non-starch macromolecules interrupted starch-chain association and reduced the long-range connectivity of the gelatinized WL network, probably through competitive hydration and steric interference (Funami et al., 2005). The decrease became less pronounced at high SC contents, suggesting that particle crowding and physical filling partly compensated for further loss of starch-network connectivity (Liu et al., 2025). The moduli remained nearly constant below approximately 10 Pa but decreased above this region, marking progressive yielding of the physical network through disruption and rearrangement of non-covalent junctions. This lower resistance to deformation favours extrusion, although excessive weakening might reduce filament self-support and printing fidelity (Hou et al., 2025; Taqdissillah et al., 2025).

Across the frequency range tested (Fig. 1b and c), *G′* remained higher than *G″*, indicating a weak-gel structure. WL exhibited the highest *G′*, which was attributed to the stable structure of its complete amylose and amylopectin networks, whereas both *G′* and *G″* decreased progressively from SC-8% to SC-

32%. At low SC content, starch -polysaccharide entanglement and hydrogen-bonding partly preserved the network, and at higher contents, molecular crowding and competition for association sites disrupted continuous starch-starch contacts (Ma et al., 2025; Tu et al., 2023). SC therefore weakened the long-range elastic network in a concentration-dependent manner rather than acting as a conventional gel-strengthening hydrocolloid.

All formulations exhibited a marked decrease in apparent viscosity with increasing shear rate (Fig. 1d), confirming pseudoplastic behavior suitable for extrusion (Kurapkienė et al., 2025). Notably, the viscosity profiles of SC-8%, SC-16%, and SC-24% were similar over most of shear-rate range, indicating a broad concentration window with comparable flow resistance. This may be attributed to the fact that the interaction between SC and the matrix tended to be balanced within this concentration range, and the network structure was relatively uniform, thus resulting in insignificant changes in viscosity. WL showed a steeper viscosity decrease at high shear, whereas SC-32% retained a higher high-shear viscosity, consistent with the greater solids content and particle crowding at the highest SC level.

Thixotropy tests revealed the structural recovery ability of various gel formulations after shearing (Wang et al., 2022). SC markedly improved structural recovery after high shear (Fig. 1e). The thixotropic recovery increased from 13.1% for WL to 16.1%, 24.6%, 28.1%, and 28.2% for SC-8%, SC-16%, SC-24%, and SC-32%, respectively. The near-identical values at 24% and 32% indicate a saturation threshold. Although SC reduced the equilibrium moduli, its hydrated polysaccharides and dispersed particles promoted rapid re-association after shear, which is advantageous for rebuilding filament integrity immediately after extrusion (Wang et al., 2023). The above results reveal the regulation law of SC on the thixotropy-recovery behavior of the material, which can provide a basis for the formulation design and rheological performance optimization of related materials.

Creep-recovery tests further distinguished elastic connectivity from compressive reinforcement (Fig. 1f). Total strain and residual deformation increased with SC content, while WL showed the greatest recovery and SC-32% the slowest recovery. These results confirm that the continuous starch-rich network became more compliant and plastic as SC increased (Wang, Jiang, et al., 2025). The contrast between lower dynamic elasticity and the higher hardness observed at high SC content indicates that particle filling and local interfacial reinforcement increased resistance to compression without restoring long-range elastic connectivity.

3.2. Collapse resistance

The morphology and diameter change after printing were shown in Fig. 2a and 3a. A gradual intensification of gel color was observed as the SC content increased from 0% to 32%. However, diameter change decreased as SC content increased from 0% to 16% and then reached a plateau at 24–32%. The initial improvement is attributed to increased solids, hydration, and particle-mediated support within the deposited filaments. Beyond 16%, the small additional change indicates diminishing returns once the composite skeleton had reached a packing threshold. Thus, moderate SC incorporation was

sufficient to improve geometric stability, while further addition mainly altered texture rather than collapse resistance (Tu et al., 2023; S. Zhang et al., 2024). In summary, SC could significantly enhance the stability of WL.**3.3. Drop resistance**

The drop test revealed a clear concentration-dependent improvement in impact resistance (Fig. 2b). WL collapsed and lost its layered architecture, indicating insufficient cohesion and interlayer support. SC-8% curled after impact, SC-16% largely retained its shape but developed a central crack, and SC-24% showed limited tilting. SC-32% preserved the printed geometry with no obvious cracking. The enhanced resistance at high SC content was consistent with increased solids loading, pore filling, and stronger local contacts between the starch-rich matrix and SC particles.

Hardness, gumminess, and chewiness described the force required to compress and orally process a semisolid food, whereas breaking force and fracturability reflected resistance to the first structural failure. These parameters were used to determine how the loss of long-range elasticity was balanced by local reinforcement in the SC-WLG composites (Fig. 3b-d). Hardness, gumminess, and chewiness remained statistically unchanged from WL to SC-16% ($p > 0.05$) but significantly at 24% and 32% SC ($p < 0.05$). Moreover, the maximum values were observed at 32% (136.55 gf, 94.11 gf, and 89.09 gf, respectively), identifying a reinforcement threshold between 16% and 24%. Below this threshold, SC remained a dispersed phase and did not form enough particle-particle or particle-matrix contacts to alter bulk compression. At 24% and above, the higher solids concentration and more continuous filler phase increased resistance to deformation (Feng et al., 2022).

The textural transition could be explained by two coupled mechanisms. First, hydroxyl- and carboxyl-rich SC macromolecules altered water partitioning and increased the immobilized-water fraction, reducing lubrication between structural elements. Second, SC particles filled voids and increased the number of local contacts within the composite skeleton. Consequently, the matrix became more densely packed even though the continuous starch network was less elastic. Similar decoupling between dynamic modulus and compressive hardness had been observed in starch-polysaccharide and starch-protein composites, where local packing and interfacial adhesion dominated large-strain deformation. In summary, SC components formed a dense hydrogen-bonded cross-linked network with starch molecules, and simultaneously regulated water distribution and densified the microstructure, ultimately achieving a synchronous increase in hardness, gumminess, and chewiness. This finding provides an important reference for the formulation design of foods for people with dysphagia.

Breaking force and fracturability followed the same threshold response (Fig. 3e and 3f). No significant differences were observed among WL, SC-8%, and SC-16%, whereas both parameters increased at 24% and 32% SC ($p < 0.05$), reaching 136.55 and 136.43 gf, respectively, at 32% SC. In this context, the higher fracturability value represents a greater force at the first fracture event rather than a more fragile structure. The results therefore indicate stronger resistance to crack initiation and propagation at high SC contents. At SC contents of at least 24%, increased interfacial contact and reversible non-covalent interactions improved stress transfer across the composite. Under compression, molecular-chain

slippage and reversible bond rupture dissipated energy, while particle filling limited crack growth (Min et al., 2023; Pan et al., 2024). These mechanisms explained the improved drop resistance and shape retention of SC-24% and SC-32%. However, the simultaneous increased in hardness and chewiness also implied a higher oral-processing demand, making IDDSI verification essential rather than assuming that greater mechanical stability automatically improved dysphagia suitability. Overall, 24–32% SC produced the strongest printed structures, whereas 8–16% SC preserved a softer texture. This concentration-dependent trade-off provided a practical formulation window for balancing shape stability against oral processing requirements.

3.5. Static stability

The experiment measured the deposition rate to reflect the effect of SC on the anti-diffusion layering ability of the WL water dispersion system. WL showed the highest deposition ratio (96.1%), indicating the poorest dispersion stability (Fig. 4b). Addition of 8% SC reduced the ratio to 87.92%, consistent with thickening and adsorption of SC polysaccharides onto starch-rich particles. At the SC-16% point, the deposition rate of the composite system rebounded to 93.93%, suggesting bridging flocculation at intermediate surface coverage, where one polysaccharide chain can adsorb onto several particles and generate larger aggregates that settle more readily (Iselau et al., 2016). Further increasing SC to 24% and 32% decreased the ratio to 86.40% and 85.98%, respectively. At these concentrations, more complete surface coverage, higher continuous-phase viscosity, and network formation suppressed particle migration. The non-monotonic response therefore reflected a transition from adsorption and bridging to steric stabilization and network immobilization.

3.6. LF-NMR analysis

The T_2 relaxation spectra and the corresponding peak area percentages of SC-WLG were presented in Fig. 4c. All samples exhibited three typical transverse relaxation peaks, with free water (T_{22}) exceeding 93% of the total peak area, indicating that the high-moisture composite gel was dominated by physically entrapped free water, consistent with previous reports on whole lotus root powder gel systems (Wang, Peng, et al., 2025). With increasing SC, the distribution of water in different states displayed significant and regular changes. The free water content first decreased and then rebounded. This fraction decreased from 94.78% in WL to 93.73% and 93.19% in SC-8% and SC-16%, respectively, while the intermediate-mobility fraction increased (Fig. 4d). The shift indicated that hydroxyl-rich SC polysaccharide expanded the hydration layer and restricted part of the mobile water through hydrogen-bonding and physical entrapment (W. Zhang et al., 2024). At 24% and 32% SC, the free water fraction increased slightly to 93.67% and 93.45%, while the immobilized water proportions stabilized at 6.30% and 6.34%. This suggests that excessive SC may interfere with the orderly formation of the continuous gel network in WL, causing the previously bound water to be released back as free water. The decrease in gel network density induced by polysaccharide excess has also been observed in other studies (Zhou et al., 2023). And this saturation was consistent with competitive hydration and disruption of the continuous starch network at high SC loading. The bound water content in all samples remained at an

extremely low level (0.03%–0.47%) and showed no obvious dose-dependent relationship. Overall, SC redistributed rather than simply bound water, and the plateau in water immobilisation paralleled the saturation in thixotropic recovery.

3.7. FT-IR analysis

All formulations exhibited the typical carbohydrate bands, and no new absorption bands appeared after SC addition (Fig. 4e), indicating that the component was stabilized predominately by non-covalent interactions rather than new covalent bonds (Ma et al., 2025; Zhang et al., 2023). The broad O-H stretching band at 3600–3200 cm^{-1} shift progressively to lower wavenumbers with increasing SC, consistent with stronger or more extensive hydrogen-bonding among starch, SC polysaccharides, proteins, and water (Kang et al., 2022; Lou et al., 2025). In contrast, the absorption peak near 2930 cm^{-1} was attributed to the C-H stretching vibration in the glucose units of starch, and the peak position and shape change little, suggesting that hydrophobic interaction was not the dominant force in the composite system (Mahmood et al., 2017). In the fingerprint region of 1200 – 900 cm^{-1}, the degree of short-range ordered structure of starch molecular chains could be characterized by semi-quantitative analysis of the intensity ratio of absorption peaks at 1047 cm^{-1} and 1022 cm^{-1} ($R_{1047}/_{1022}$) (Colussi et al., 2014; S. Wang et al., 2020). The $R_{1047}/_{1022}$ ratio decreased with increasing SC, indicating reduced short-range order of starch chains. SC macromolecules therefore interfered with starch chain reassociation and double-helix formation while participating in a broader hydrogen-bonded composite network (S. Wang et al., 2020). This distinction helped explain why SC weakened the starch-rich elastic network but improved local packing and recovery.

Protein secondary structure composition was obtained by baseline correction, deconvolution, second derivative fitting, and peak shape fitting of the amide I band (1600–1700 cm^{-1}) (Han et al., 2015). WL protein was mainly composed of β-turn, β-sheet, and α-helix conformations without random coil (Z. Zhang et al., 2021), indicating that gelatinization and lyophilization preserved a relatively regular ordered conformation through strong hydrogen bonds and hydrophobic interactions (Jiang et al., 2025). Thermal and dehydration treatments promoted conformational rearrangement toward more stable ordered structures, inhibiting the random coil formation (Griebenow et al., 1995). Nevertheless, the deficiency in flexible segments and random coil might reduce system flexibility and ductility, potentially compromising extrusion molding and interlayer adhesion in 3D printing. Curve fitting of the amide I band showed concentration-dependent rearrangement of the protein fraction (Fig. 4f). WL was dominated by β-turn, β-sheet, and α-helix structures. At 8% SC, the relative proportions of β-sheet and α-helix increased and β-turn decreased, suggesting enhanced local ordering at low addition. At 16–24% SC, β-turn gradually increased as steric crowding and polysaccharide-protein association promoted partial rearrangement of the ordered structures (Guo et al., 2024). At 32% SC, the α-helix fraction decreased further and β-turn increased, consistent with crowding-induced helix destabilization and a more flexible protein conformation (Yue et al., 2011). This change reflected the transition of protein conformation from highly ordered to flexible relaxation at high addition levels, revealing the interference of excessive exogenous components on the ordered assembly of proteins.

3.8. Molecular interaction force

As shown in Fig. 4g, the intermolecular interactions assay indicated that hydrophobic interactions and disulfide bonds contributed more to protein-network stabilization than ionic bonds and hydrogen bonds. SC addition decreased the apparent contributions assigned to ionic bonds and hydrogen bonds significantly ($p < 0.05$), likely due to SC polysaccharide competed for water and protein binding sites, thereby changing the association pattern among proteins (Wang et al., 2024). This phenomenon was consistent with the reported that polysaccharides weaken hydrogen bonds in plant protein systems, suggesting that polysaccharides incorporation altered proteins non-covalent association through intermolecular competition (Yang et al., 2018).

The contribution assigned to hydrophobic interactions increased with SC and reached a maximum at 24%, suggesting partial protein rearrangement and exposure of hydrophobic residues in the altered microenvironment (Q. Zhang et al., 2021; Zhao et al., 2024). The response plateaued or decreased slightly at 32%, consistent with excessive crowding and reduced molecular mobility. Importantly, the decrease in protein-protein hydrogen-bond contribution did not contradict the FTIR red shift. The intermolecular interactions assay probed interactions stabilizing the soluble protein fraction, whereas FTIR reflected hydrogen-bonding across the entire starch-polysaccharide-protein-water matrix. Together, the results indicated that SC redistributed hydrogen bonds from protein-protein contacts toward heterotypic matrix interactions while strengthening hydrophobic association, with 24% SC marking the most balanced interfacial state.

3.9. CLSM analysis

CLSM images (Fig. 5a) were acquired using Nile Blue and Rhodamine B to label SC and proteins, respectively. At low SC concentrations, the blue channel revealed uniformly dispersed SC particles as fine dots within WL starch matrix, with intimate interfacial contact between the two components. Increasing the SC level led to larger and denser fluorescent clusters, exhibiting localized agglomeration, although the particle surfaces remained partially or completely encapsulated by the starch matrix, indicating favourable physical compatibility (Qiu et al., 2024; Shao et al., 2023). In the red channel, proteins were initially appeared as small spots localized at the starch-SC interfaces. With rising SC content, the red fluorescence progressively intensified and transformed from a punctuate distribution to a more continuous phase that interpenetrated with the starch-rich matrix (Du & Meng, 2025). This protein phase became increasingly continuous with higher SC levels, and the resulting interpenetrating network among the starch, SC and protein phases collectively provided a microstructural foundation that underpinned both the smooth extrudability and shape retention observed during 3D printing.

3.10. Optical microscopy analysis

Optical microscopy was used to assess starch swelling and the continuity of the starch-rich phase after gelatinization (Fig. 5b). The addition amount of SC could significantly alter the compactness of the gel network in the system, and this structural difference was closely related to the gelatinization degree of

starch. In WL, most starch granules were strongly swollen or disrupted, producing a relatively continuous gelatinized matrix (Nilsson et al., 2023). At low SC ratio, SC proteins and dietary fibers adsorbed onto starch surfaces and introduced mild steric hindrance, but the gelatinized phase remained largely continuous and no marked phase separation was observed (Souza Almeida & Kawazoe Sato, 2019). At higher SC contents, more residual or incompletely swollen starch granules and SC-rich aggregates were visible. Encapsulation and competition for water likely restricted starch hydration, swelling, and rupture, thereby reducing the continuity of the starch-rich phase (Huang et al., 2025; Min et al., 2023; Xue et al., 2025; Y. Zhang et al., 2024). Thus, SC progressively inhibited complete starch gelatinization and weakened long-range starch-network connectivity, in agreement with the lower dynamic moduli. This observation did not preclude densification of the overall composite skeleton because un-gelatinized particles and SC solids could fill voids and increase local packing, as shown by SEM.

3.11. Scanning electron microscopy

The SEM images clearly showed a progressive reduction in pore size as SC increased from 0% to 32% (Fig. 6), with the most compact freeze-dried skeletons observed at 24% and 32% SC. At low addition, SC occurred mainly as isolated particles or small aggregates and provided limited void filling. Meanwhile, limited by intermolecular forces, the hydrogen bonds in the system were inhibited by the dilution effect, and the ionic bonds were significantly weakened by the charge shielding effect brought by acidic polysaccharides, resulting in low overall intermolecular binding strength (Liu et al., 2023). At higher addition, SC polysaccharides, proteins, and fibres occupied spaces within the WL matrix and increased the density of local contacts, converting larger connected pores into smaller, more uniform voids (Xu et al., 2022). Hydrogen-bonding, hydrophobic association, and disulfide-linked protein contacts further stabilized this packed skeleton (Han et al., 2023; Zheng et al., 2020). Optical microscopy and SEM therefore captured complementary aspects of the same mechanism. SC reduced the extent and continuity of starch gelatinization in the hydrated state, but the added solids filled voids and densified the overall composite after gel formation. This multiscale decoupling explained the simultaneous decrease in G', increase in creep deformation, improvement in thixotropic recovery, and rise in hardness and impact resistance at high SC contents. The structure-function relationship was therefore governed by a transition from a starch-continuous gel to a densely packed, particle-reinforced composite.

3.12. *In vitro* digestion

The glucose release curves of the composite systems with different SC levels were presented in Fig. 7a. All samples exhibited glucose release during the first 20 min, followed by a slower phase and an apparent plateau after 120 min, consistent with the typical pattern of *in vitro* starch-hydrolysis kinetics (L. Wang et al., 2020). SC reduced glucose release throughout digestion. At 180 min, glucose release decreased from 21.06 mg for WL to13.50 mg for SC-32%, a reduction of 35.9%. The hydrolysis curves showed little separation during the first 20 min, but divergence became pronounced thereafter (Fig. 7b). Final starch hydrolysis decreased from13.03% for WL to was 9.33% for SC-32%, corresponding to a

28.4% reduction. The delayed phase suggested that SC mainly restricted sustained enzyme access and diffusion rather than eliminating the rapidly accessible starch fraction at the onset of digestion.

The contents of rapidly digestible starch (RDS), slowly digestible starch (SDS), and resistant starch (RS) in different samples were shown in Fig. 7c. WL exhibited the highest RDS content (4.09%).RDS decreased with increasing SC, which was consistent with the reduction in RDS observed in noodles supplemented with *Hericium erinaceus* powder (L. Wang et al., 2020). SDS varied only slightly and showed no significant difference among formulations ($p > 0.05$). RS increased significantly after SC addition. The higher RS fraction was consistent with reduced starch gelatinization, lower short-range order rearrangement during processing, physical encapsulation by SC-rich domains, and restricted amylase diffusion through the packed composite matrix. Although resistant starch could be fermented in the colon, the physiological consequences of the increase observed here required confirmation in biological models (Lu et al., 2021).

HI and eGI values decreased significantly with increasing SC (Fig. 7d). The eGI value of the WL group was 65.60, within the medium GI range (56–69), whereas. SC-24% decreased to 57.07 and SC-32% to 52.76. The latter value was below the conventional low-GI threshold of 55. Because these values were derived from an *in vitro* model, they indicate attenuated glycemic potential rather than a clinically established glycemic index. The reduction was attributed to the combined effects of incomplete starch gelatinization, lower enzyme accessibility, and the diffusion barrier created by the SC-reinforced composite skeleton.

3.13. IDDSI assessment

The IDDSI framework provided a global standardized system for classifying foods suitable for individuals with dysphagia (Cichero et al., 2016). The fork-pressure, fork-drip, and spoon-tilt tests were used to evaluate whether the printed gels met qualitative IDDSI criteria for texture-modified foods (Fig. 8). All formulations were readily compressed with a fork without observable blanching on the fingertips. Increasing SC reduced the extent of deformation, consistent with the texture-analysis results, but the samples remained compressible. None of the formulations dripped through the fork tines, and all slid from the spoon as cohesive masses without leaving substantial residue. On the basis of the tests performed, the formulations met the qualitative criteria used here for IDDSI Level 5 (Minced & Moist) (Cichero et al., 2016), which was appropriate for individuals with limited chewing ability.

4. Conclusion

SC produced a concentration-dependent transition in WL gels from a starch-continuous network to a densely packed, particle-reinforced composite. Increasing SC weakened long-range elasticity and increased creep deformation by disrupting starch-chain association and limiting complete gelatinization. At the same time, hydrated polysaccharides, proteins, and fibers enhanced post-shear rebuilding, filled structural voids, and strengthened local interfaces. Above a threshold of approximately 24% SC, these effects increased hardness, impact resistance, and shape retention despite the lower dynamic moduli.

The packed multicomponent structure also restricted enzyme access, decreasing 180-min starch hydrolysis by 28.4% and lowering eGI from 65.60 to 52.76 at 32% SC. All formulations met the qualitative IDDSI Level 5 criteria evaluated in this study. The central mechanistic insight is therefore the decoupling of long-range starch-network elasticity from local particle-driven reinforcement, which enables simultaneous control of printability, texture, and starch digestibility. SC-WLG provides a promising platform for dysphagia-oriented 3D-printed foods, although sensory acceptability, nutrient bioavailability, clinical swallowing safety, and postprandial glycemic responses should be validated in future studies.

CRediT authorship contribution statement

Xuanzi Liu and, Xuanxuan Cao, Jinfeng Wang: Investigation, Methodology, Data curation, Writing-original draft. Huanhuan Liu and Hao Dong: Data curation, Project administration. Yi Yang: Conceptualization, Supervision, Validation. Xueyu Jiang: Conceptualization, Methodology, Funding acquisition, Writing-review & editing, Supervision. All authors have read and agreed to the published version of the manuscript.

Declarations

CRediT authorship contribution statement

Xuanzi Liu and, Xuanxuan Cao, Jinfeng Wang: Investigation, Methodology, Data curation, Writing-original draft. Huanhuan Liu and Hao Dong: Data curation, Project administration. Yi Yang: Conceptualization, Supervision, Validation. Xueyu Jiang: Conceptualization, Methodology, Funding acquisition, Writing-review & editing, Supervision. All authors have read and agreed to the published version of the manuscript.

Funding

This work was supported by the Science and Technology Department of Hubei Province grant (2025DJB014 and 2025BBB041).

Data availability

Data will be made available on request.

Declaration of competing interest

The authors declare no competing financial interest.

References

1. Cichero, J. A. Y., Lam, P., Steele, C. M., Hanson, B., Chen, J., Dantas, R. O., Duivestein, J., Kayashita, J., Lecko, C., Murray, J., Pillay, M., Riquelme, L., & Stanschus, S. (2016, 2016/12/02). Development of

International Terminology and Definitions for Texture-Modified Foods and Thickened Fluids Used in Dysphagia Management: The IDDSI Framework. *Dysphagia*. https://doi.org/10.1007/s00455-016-9758-y

2. Colussi, R., Pinto, V. Z., El Halal, S. L. M., Vanier, N. L., Villanova, F. A., Marques e Silva, R., da Rosa Zavareze, E., & Dias, A. R. G. (2014, 2014/02/18). Structural, morphological, and physicochemical properties of acetylated high-, medium-, and low-amylose rice starches. *Carbohydrate Polymers*. https://doi.org/10.1016/j.carbpol.2013.12.070
3. Du, L., & Meng, Z. (2025, 2025/01/04). Whipped foams from Pickering O/W/O emulsion gel-based fat analogue: Thermal reversibility, oral tribology, and 3D printing characteristics dominated by fat crystals. *Food Hydrocolloids*. https://doi.org/10.1016/j.foodhyd.2025.111050
4. Feng, L., Wu, J., Cai, L., Li, M., Dai, Z., Li, D., Liu, C., & Zhang, M. (2022, 2022/06/06). Effects of different hydrocolloids on the water migration, rheological and 3D printing characteristics of β-carotene loaded yam starch-based hydrogel. *Food Chemistry*. https://doi.org/10.1016/j.foodchem.2022.133422
5. Funami, T., Kataoka, Y., Omoto, T., Goto, Y., Asai, I., & Nishinari, K. (2005, 2005/01/01). Effects of non-ionic polysaccharides on the gelatinization and retrogradation behavior of wheat starch. *Food Hydrocolloids*. https://doi.org/10.1016/j.foodhyd.2004.04.024
6. Griebenow, K, Klibanov, & M, A. (1995, 1995/11/21). Lyophilization-induced reversible changes in the secondary structure of proteins. *Proceedings of the National Academy of Sciences of the United States of America*.
7. Guo, Y., Lin, K., Wang, Y., Dong, P., Du, P., Cao, J., Cheng, Y., Cheng, F., Yun, S., & Feng, C. (2024, 2024/11/12). Investigation on the interfacial and emulsion stabilized behavior of dextran/ferritin/resveratrol composite nanoparticles. *International Journal of Biological Macromolecules*. https://doi.org/10.1016/j.ijbiomac.2024.137533
8. Han, X., Liang, Q., Rashid, A., Qayum, A., Rehman, A., Zhong, M., Sun, Y., Liu, Y., Ma, H., Miao, S., & Ren, X. (2023, 2023/12/05). The effects of different hydrocolloids on lotus root starch gelatinization and gels properties. *International Journal of Biological Macromolecules*. https://doi.org/10.1016/j.ijbiomac.2023.128562
9. Han, Y., Wang, J., Li, Y., Hang, Y., Yin, X., & Li, Q. (2015, 2015/04/21). Circular dichroism and infrared spectroscopic characterization of secondary structure components of protein Z during mashing and boiling processes. *Food Chemistry*. https://doi.org/10.1016/j.foodchem.2015.04.053
10. Hou, J., Jiang, Z., Wang, J., Xu, L., Zhang, H., Li, H., Yu, X., Xia, N., Ma, Y., Rayan, A. M., & Ghamry, M. (2025, 2025/03/14). Micronutrient supplemented dysphagia food: Rheology and β-carotene delivery of 3D printing egg yolk-carboxymethyl cellulose emulsion gels. *Food Research International*. https://doi.org/10.1016/j.foodres.2025.116213
11. Huang, J., Ying, C., Li, X., Kuang, J., Li, J., Huang, T., & Li, J. (2025, 2025/01/22). Study on structure, properties and formation mechanism of cassava starch-faba bean protein heat-induced gel. *International Journal of Biological Macromolecules*. https://doi.org/10.1016/j.ijbiomac.2025.140216

12. Iselau, F., Phan Xuan, T., Trefalt, G., Matic, A., Holmberg, K., & Bordes, R. (2016, 2016/11/09). Formation and relaxation kinetics of starch–particle complexes†. *Soft Matter*. https://doi.org/10.1039/c6sm01312k
13. Jiang, F., Sun, B., Liu, Y., Wang, Z., Zhang, Z., Ma, X., Yu, H., Dai, W., & Lyu, B. (2025, 2025/10/26). The modification of β-conglycinin by Polygonatum sibiricum polysaccharide through covalent and non-covalent interactions: structure and processing characteristics. *International Journal of Biological Macromolecules*. https://doi.org/10.1016/j.ijbiomac.2025.148552
14. Kang, X., Jia, S., Gao, W., Wang, B., Zhang, X., Tian, Y., Sun, Q., Atef, M., Cui, B., & Abd El-Aty, A. M. (2022, 2022/02/04). The formation of starch-lipid complexes by microwave heating. *Food Chemistry*. https://doi.org/10.1016/j.foodchem.2022.132319
15. Kurapkienė, A., Vinauskienė, R., Eisinaitė, V., & Leskauskaitė, D. (2025, 2025/04/04). Development of Meat-Based Formulations for 3D Printed Products Oriented to Dysphagia Diet. *Journal of Texture Studies*. https://doi.org/10.1111/jtxs.70015
16. Liu, W., Chen, L., McClements, D. J., Zou, Y., Chen, G., & Jin, Z. (2023, 2023/11/09). Vanillin-assisted preparation of chitosan-betaine stabilized corn starch gel: Gel properties and microstructure characteristics. *Food Hydrocolloids*. https://doi.org/10.1016/j.foodhyd.2023.109510
17. Liu, Y., Li, X., Chen, L., Feng, F., Sun, C., Xu, Y., Sun, X., Li, M., Sun, Q., Xu, X., Xie, F., & Wang, Y. (2025, 2025/09/24). Curdlan modulates potato starch gelatinization and gelation: Mechanisms of interaction, structural enhancement, and texture improvement in hydrogel foods. *Food Hydrocolloids*. https://doi.org/10.1016/j.foodhyd.2025.112033
18. Liu, Z., Chen, X., Li, H., Chitrakar, B., Zeng, Y., Hu, L., & Mo, H. (2024, 2024/04/07). 3D printing of nutritious dysphagia diet: Status and perspectives. *Trends in Food Science & Technology*. https://doi.org/10.1016/j.tifs.2024.104478
19. Lou, F., Guo, Y., Zhang, S., Sun, F., Liu, J., Jiang, L., Guo, Z., & Wang, Z. (2025, 2025/03/18). Synergistic enhancement of 3D printing performance in soybean protein isolate gel inks by Ionic/nonionic polysaccharides: A network rearrangement mechanism revealed by rheology and the sequence of physical processes analysis. *Food Hydrocolloids*. https://doi.org/10.1016/j.foodhyd.2025.111352
20. Lu, X., Brennan, M. A., Guan, W., Zhang, J., Yuan, L., & Brennan, C. S. (2021, 2021/03/30). Enhancing the Nutritional Properties of Bread by Incorporating Mushroom Bioactive Compounds: The Manipulation of the Pre-Dictive Glycaemic Response and the Phenolic Properties. *Foods*. https://doi.org/10.3390/foods10040731
21. Ma, Y., Shen, R., Wang, Y., Wang, X., Tian, X., & Wang, W. (2025, 2025/02/28). Mechanical properties of myofibrillar protein-cellulose nanofibril composite gels: Role of protein concentration and network structure. *Food Hydrocolloids*. https://doi.org/10.1016/j.foodhyd.2025.111311
22. Mahmood, K., Kamilah, H., Shang, P. L., Sulaiman, S., Ariffin, F., & Alias, A. K. (2017, 2017/05/20). A review: Interaction of starch/non-starch hydrocolloid blending and the recent food applications. *Food Bioscience*. https://doi.org/10.1016/j.fbio.2017.05.006

23. Min, C., Zhang, C., Cao, Y., Li, H., Pu, H., Huang, J., & Xiong, Y. L. (2023, 2023/03/30). Rheological, textural, and water-immobilizing properties of mung bean starch and flaxseed protein composite gels as potential dysphagia food: The effect of Astragalus polysaccharide. *International Journal of Biological Macromolecules*. https://doi.org/10.1016/j.ijbiomac.2023.124236
24. Nilsson, K., Johansson, M., Sandström, C., Eriksson Röhnisch, H., Hedenqvist, M. S., & Langton, M. (2023, 2023/01/19). Pasting and gelation of faba bean starch-protein mixtures. *Food Hydrocolloids*. https://doi.org/10.1016/j.foodhyd.2023.108494
25. Nuinamwong, S., Sermwittayawong, D., Sukpondma, Y., Tansakul, C., Purintrapibal, Y., & Decha, N. (2024, 2024/08/03). Extraction, characterization, antioxidant, and antidiabetic activities of ethanolic extracts from the split gill mushroom (Schizophyllum commune). *Food Bioscience*. https://doi.org/10.1016/j.fbio.2024.104857
26. Pan, W., Qi, X., Huang, Z., Shen, M., Wen, H., & Xie, J. (2024, 2024/10/02). Effect of three polysaccharides with different charge characteristics on the properties of highland barley starch gel. *International Journal of Biological Macromolecules*. https://doi.org/10.1016/j.ijbiomac.2024.136267
27. Qiu, R., Qiu, G., Zhao, P., Awais, M., Fan, B., Huang, Y., Tong, L., Wang, L., Liu, L., & Wang, F. (2024, 2024/03/30). Regulation of rheological properties of soy protein isolate-beeswax based bigel inks for high-precision 3D printing. *Food Hydrocolloids*. https://doi.org/10.1016/j.foodhyd.2024.110052
28. Shao, Y., Jiao, R., Wu, Y., Xu, F., Li, Y., Jiang, Q., Zhang, L., & Mao, L. (2023, 2023/01/08). Physicochemical and functional properties of the protein–starch interaction in Chinese yam. *Food Science & Nutrition*. https://doi.org/10.1002/fsn3.3189
29. Souza Almeida, F., & Kawazoe Sato, A. C. (2019, 2019/03/26). Structure of gellan gum-hydrolyzed collagen particles: Effect of starch addition and coating layer. *Food Research International*. https://doi.org/10.1016/j.foodres.2019.03.057
30. Taqdissillah, D., Irsyad, M., & Whulanza, Y. (2025). Development of sago starch-alginate hydrogels for extrusion-based 3D food printing. *Eastern-European Journal of Enterprise Technologies*, *4*(11 (136)), 33–40. https://doi.org/10.15587/1729-4061.2025.336896
31. Tu, J., Adhikari, B., Brennan, M. A., Cheng, P., Bai, W., & Brennan, C. S. (2023, 2023/01/21). Interactions between sorghum starch and mushroom polysaccharides and their effects on starch gelatinization and digestion. *Food Hydrocolloids*. https://doi.org/10.1016/j.foodhyd.2023.108504
32. Wang, H., Zhang, J., Rao, P., Zheng, S., Li, G., Han, H., Chen, Y., & Xiang, L. (2024, 2024/09/01). Mechanistic insights into the interaction of Lycium barbarum polysaccharide with whey protein isolate: Functional and structural characterization. *Food Chemistry*. https://doi.org/10.1016/j.foodchem.2024.141080
33. Wang, J., Jiang, X., Gan, H., Li, S., Peng, K., Sun, Y., Ma, M., & Yi, Y. (2025, 2025/06/09). Complexation-driven 3D printable whey protein-lotus root composite gels for dysphagia foods. *Carbohydrate Polymers*. https://doi.org/10.1016/j.carbpol.2025.123864
34. Wang, J., Jiang, X., Gan, H., Li, S., Wang, H., & Yi, Y. (2026, 2026/07/08). Tailoring dysphagia-friendly 3D printed starch-based gels: olive oil modulation of lotus root-whey protein inks. *npj Science of*

Food. https://doi.org/10.1038/s41538-026-00979-1

35. Wang, J., Peng, K., Sun, Y., Jiang, X., & Yi, Y. (2025, 2025/03/17). 3D printing performance of whole lotus root powder and lotus root starch. *International Journal of Biological Macromolecules*. https://doi.org/10.1016/j.ijbiomac.2025.142156
36. Wang, L., Tian, Y., Chen, Z., & Chen, J. (2020, 2020/12/12). Effects of Hericium erinaceus powder on the digestion, gelatinization of starch, and quality characteristics of Chinese noodles. *Cereal Chemistry*. https://doi.org/10.1002/cche.10387
37. Wang, N., Wu, L., Yang, J., You, Y., Zhang, F., Kan, J., & Zheng, J. (2023, 2023/10/20). Lotus starch/bamboo shoot polysaccharide composite system treated via ultrasound: Pasting, gelling properties and multiscale structure. *Food Research International*. https://doi.org/10.1016/j.foodres.2023.113605
38. Wang, S., Wu, T., Cui, W., Liu, M., Wu, Y., Zhao, C., Zheng, M., Xu, X., & Liu, J. (2020, 2020/09/25). Structure and in vitro digestibility on complex of corn starch with soy isoflavone. *Food Science & Nutrition*. https://doi.org/10.1002/fsn3.1896
39. Wang, X., Zhang, M., Mujumdar, A. S., & Li, J. (2022, 2022/12/27). Easy-to-swallow mooncake using 3D printing: Effect of oil and hydrocolloid addition. *Food Research International*. https://doi.org/10.1016/j.foodres.2022.112404
40. Wunjuntuk, K., Ahmad, M., Techakriengkrai, T., Chunhom, R., Jaraspermsuk, E., Chaisri, A., Kiwwongngam, R., Wuttimongkolkul, S., & Charoenkiatkul, S. (2021, 2021/10/12). Proximate composition, dietary fibre, beta-glucan content, and inhibition of key enzymes linked to diabetes and obesity in cultivated and wild mushrooms. *Journal of Food Composition and Analysis*. https://doi.org/10.1016/j.jfca.2021.104226
41. Xu, J., Zou, Y., Guo, L., Lin, J., Jiang, Z., & Zheng, Q. (2022, 2022/12/22). Rheological and microstructural properties of polysaccharide obtained from the gelatinous Tremella fuciformis fungus. *International Journal of Biological Macromolecules*. https://doi.org/10.1016/j.ijbiomac.2022.12.214
42. Xue, H., Gao, H., Fang, S., Hao, Z., Liao, X., & Tan, J. (2025, 2025/01/06). Understanding the role of Radix Paeoniae Alba polysaccharide for corn starch gel amelioration: Physicochemical, structural, and digestive properties. *International Journal of Biological Macromolecules*. https://doi.org/10.1016/j.ijbiomac.2025.139564
43. Yang, C., Zhong, F., Douglas Goff, H., & Li, Y. (2018, 2018/12/13). Study on starch-protein interactions and their effects on physicochemical and digestible properties of the blends. *Food Chemistry*. https://doi.org/10.1016/j.foodchem.2018.12.028
44. Yue, Y., Liu, J., Fan, J., & Yao, X. (2011, 2011/05/20). Binding studies of phloridzin with human serum albumin and its effect on the conformation of protein. *Journal of Pharmaceutical and Biomedical Analysis*. https://doi.org/10.1016/j.jpba.2011.05.018
45. Zhang, C., Wang, C.-S., Girard, M., Therriault, D., & Heuzey, M.-C. (2023, 2023/10/24). 3D printed protein/polysaccharide food simulant for dysphagia diet: Impact of cellulose nanocrystals. *Food*

Hydrocolloids. https://doi.org/10.1016/j.foodhyd.2023.109455

46. Zhang, Q., Zhou, Y., Yue, W., Qin, W., Dong, H., & Vasanthan, T. (2021, 2021/01/14). Nanostructures of protein-polysaccharide complexes or conjugates for encapsulation of bioactive compounds. *Trends in Food Science & Technology*. https://doi.org/10.1016/j.tifs.2021.01.026
47. Zhang, S., Liu, Y., Sun, T., Liu, H., & Wang, D. (2024, 2024/05/06). The Effects of Tremella fuciformis Polysaccharide on the Physicochemical, Multiscale Structure and Digestive Properties of Cyperus esculentus Starch. *Foods*. https://doi.org/10.3390/foods13091425
48. Zhang, W., Ye, X., Zhao, J., Song, J., Jiao, J., Ou, X., & Xie, J. (2024, 2024/12/30). Preparation and texture assessment of purple red rice bran anthocyanins-rice starch based dysphagia food masses. *Food Research International*. https://doi.org/10.1016/j.foodres.2024.115534
49. Zhang, Y., Yang, B., Zhou, S., Han, X., Jiang, Y., Zhou, X., Yang, X., & Zhao, J. (2024, 2024/08/13). Pasting, rheology, structural properties and in vitro digestibility of potato starch complexes co-gelatinized with squash polysaccharides. *Food Bioscience*. https://doi.org/10.1016/j.fbio.2024.104932
50. Zhang, Z., Chen, X., Liu, X., Liu, W., Liu, Q., Huang, J., Zhang, L., & Hu, H. (2021, 2021/10/05). Effect of salt ions on mixed gels of wheat gluten protein and potato isolate protein. *LWT - Food Science and Technology*. https://doi.org/10.1016/j.lwt.2021.112564
51. Zhao, Y., Wang, D., Xu, J., Tu, D., Zhuang, W., & Tian, Y. (2024, 2024/01/27). Effect of polysaccharide concentration on heat-induced Tremella fuciformis polysaccharide-soy protein isolation gels: Gel properties and interactions. *International Journal of Biological Macromolecules*. https://doi.org/10.1016/j.ijbiomac.2024.129782
52. Zheng, L., Wang, Z., Kong, Y., Ma, Z., Wu, C., Regenstein, J. M., Teng, F., & Li, Y. (2021, 2021/01/01). Different commercial soy protein isolates and the characteristics of Chiba tofu. *Food Hydrocolloids*. https://doi.org/10.1016/j.foodhyd.2020.106115
53. Zheng, M., Lin, Y., Wu, H., Zeng, S., Zheng, B., Zhang, Y., & Zeng, H. (2020, 2020/01/20). Water migration depicts the effect of hydrocolloids on the structural and textural properties of lotus seed starch. *Food Chemistry*. https://doi.org/10.1016/j.foodchem.2020.126240
54. Zhou, J., Cen, Q., Tie, H., Hui, F., Qian, R., Ying, X., Fan, J., & Zeng, X. (2026, 2026/03/02). Effects of Ganoderma-lucidum-fermented sugarcane bagasse–soybean residue substrate on the quality and starch digestibility of steamed bread. *LWT - Food Science and Technology*. https://doi.org/10.1016/j.lwt.2026.119185
55. Zhou, T.-Q., Wang, X.-C., Gao, L.-Y., Yan, J.-N., & Wu, H.-T. (2023, 2023/10/12). Construction and properties of curdlan gum/gellan gum binary composite gel system. *Food Hydrocolloids*. https://doi.org/10.1016/j.foodhyd.2023.109391

Figures

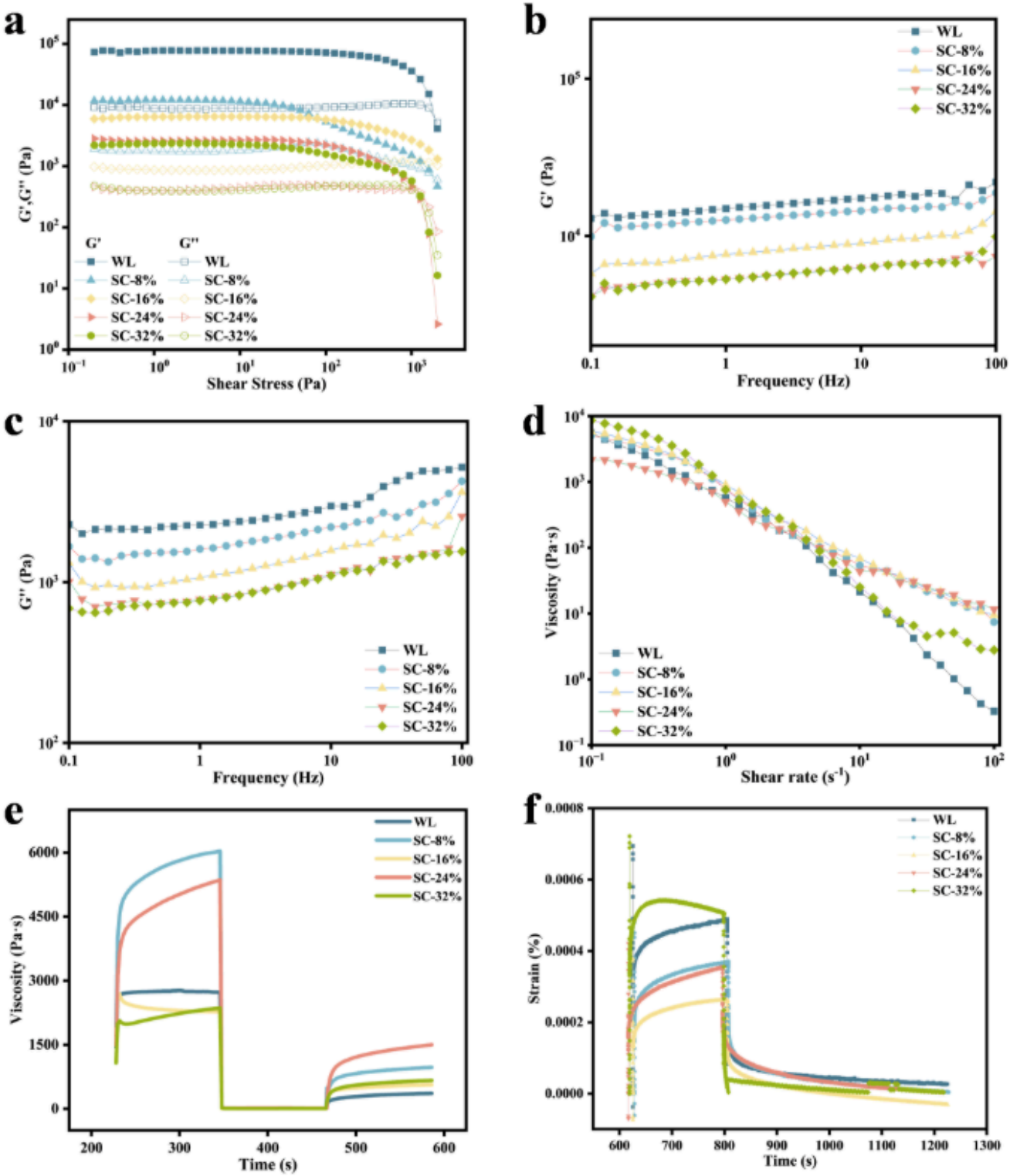


Figure 1

Rheological characteristics of SC-WLG: (a) Amplitude sweep; (b) *G*′, (c) *G*″ during frequency sweeps; (d) Shear-thinning behavior, (e) Thixotropic recovery rate, and (f) Creep-recovery analysis of samples.

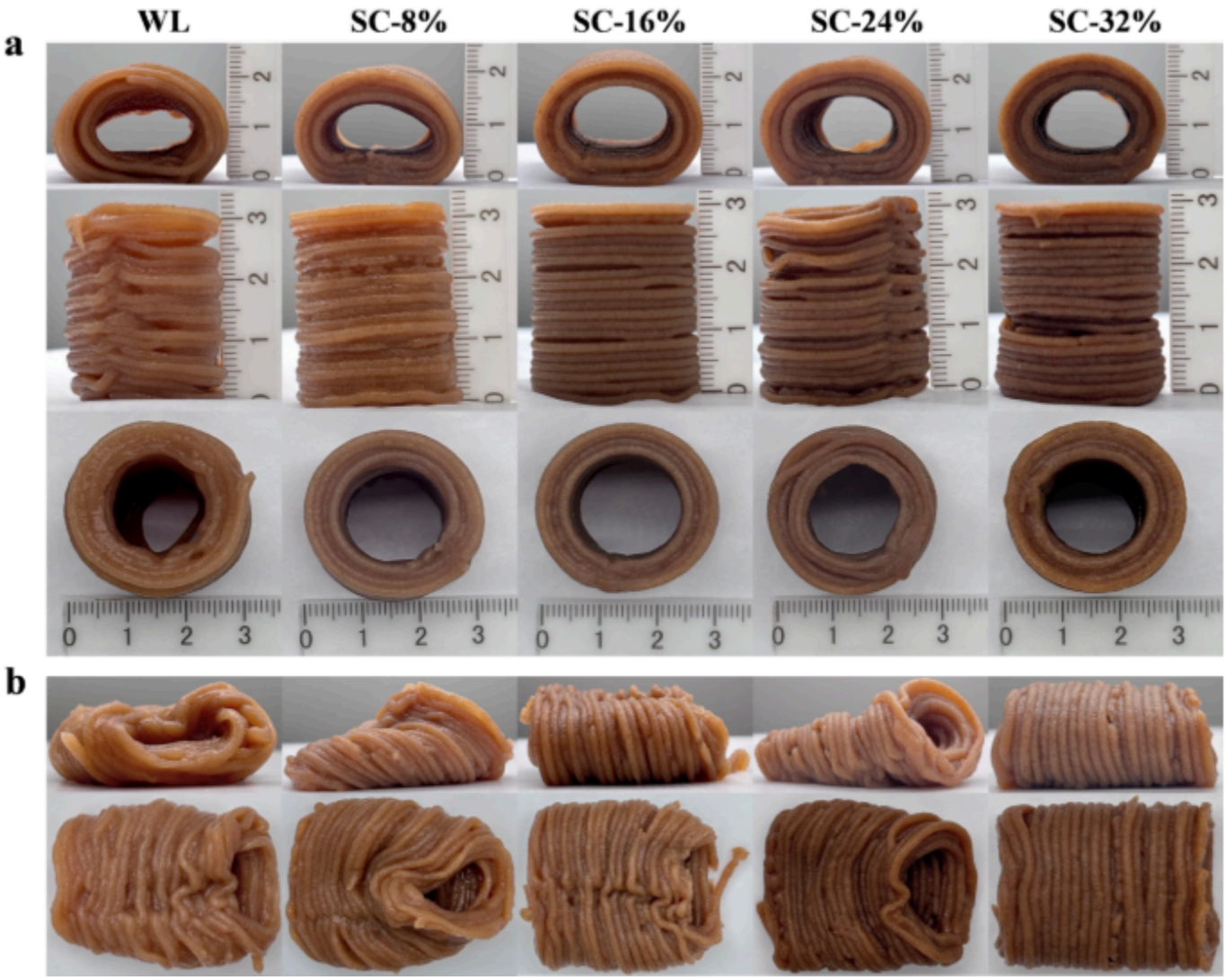


Figure 2

Structural stability of 3D-printed SC-WLG: (a) Morphology during the collapse test; (b) Front and top views after a 50-cm drop.

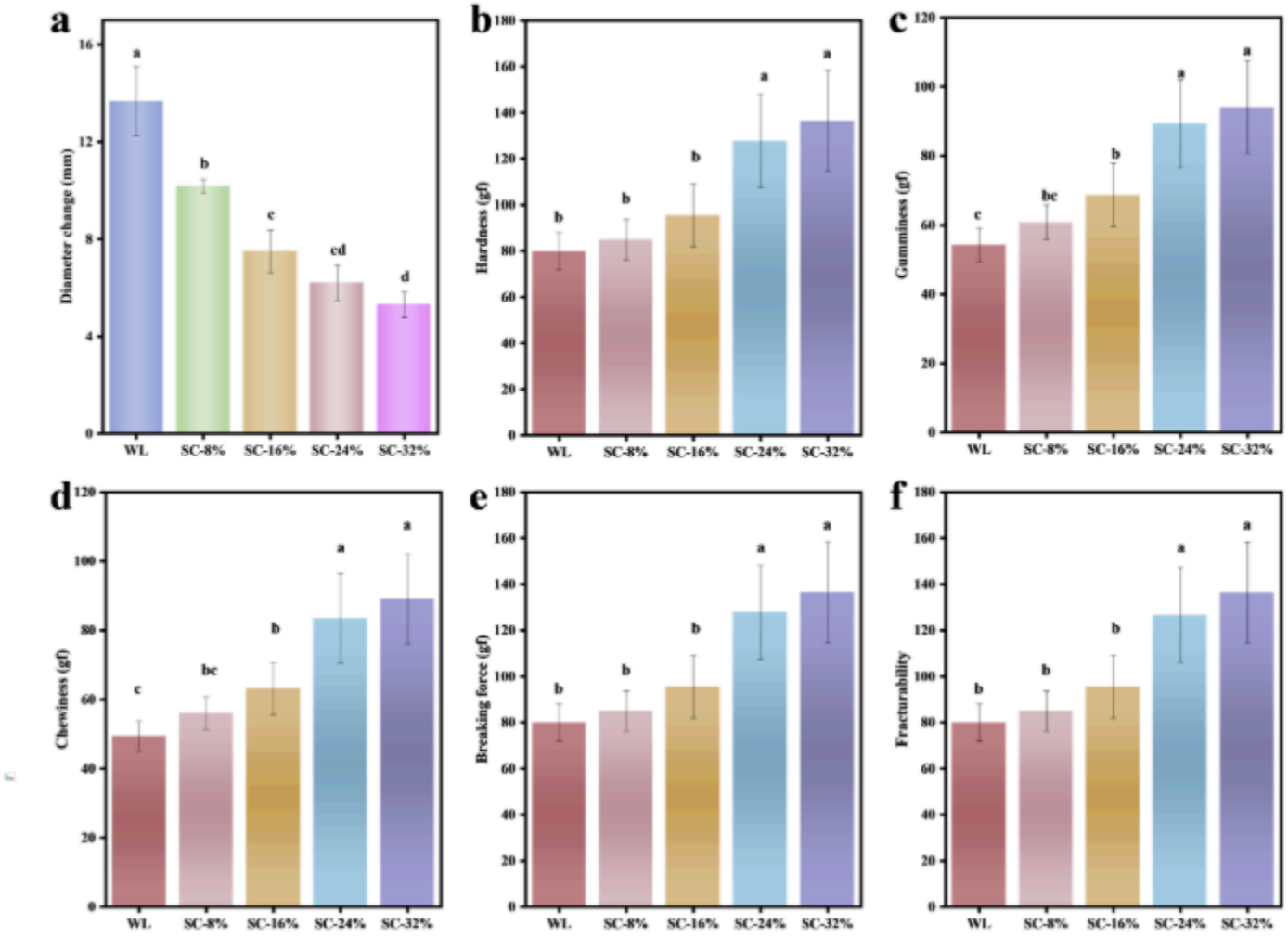


Figure 3

Collapse deformation and textural properties of SC-WLG: (a) Collapse diameter change; (b) Hardness; (c) Breaking force; (d) Fracturability; (e) Gumminess; and (f) Chewiness of SC-WLG.

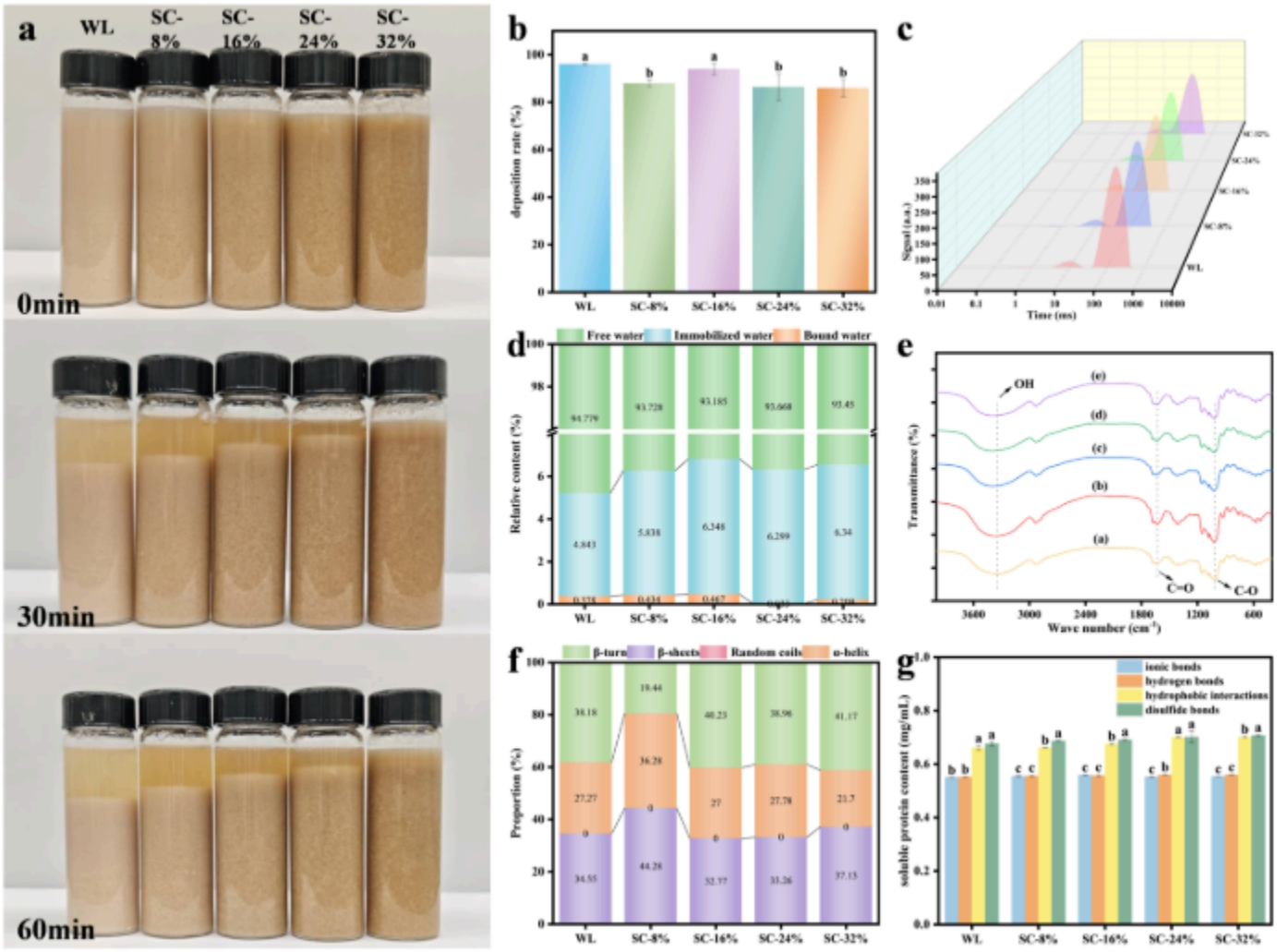


Figure 4

Physicochemical characterization of SC-WLG: (a) Static stratification observation; (b) Deposition rate; (c) LF-NMR relaxation distributions; (d) Corresponding peak area; (e) FT-IR spectra; (f) Relative content of protein secondary structures; (g) Molecular interactions.

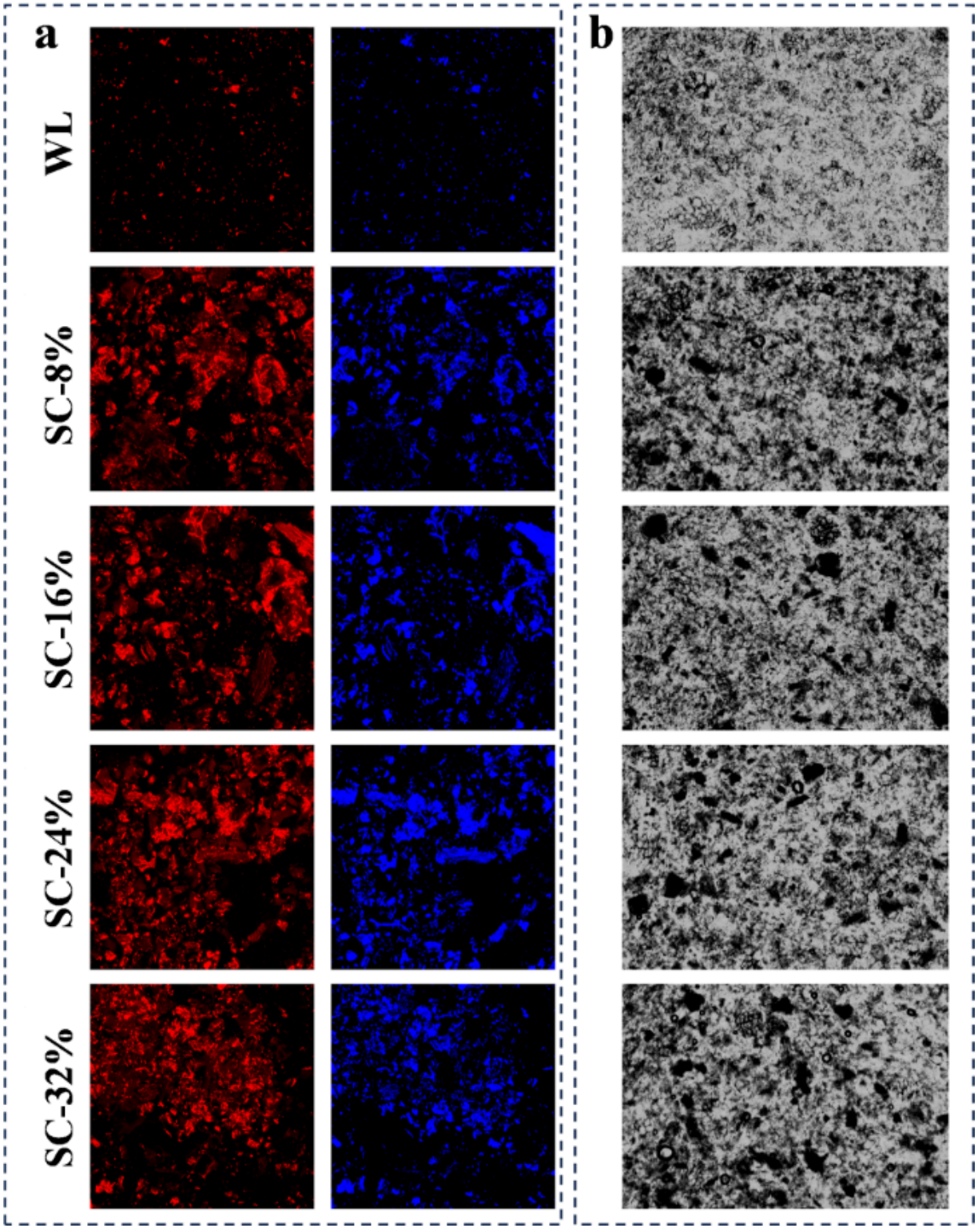


Figure 5

Microstructure of SC-WLG: (a) CLSM images and (b) Optical microscope images.

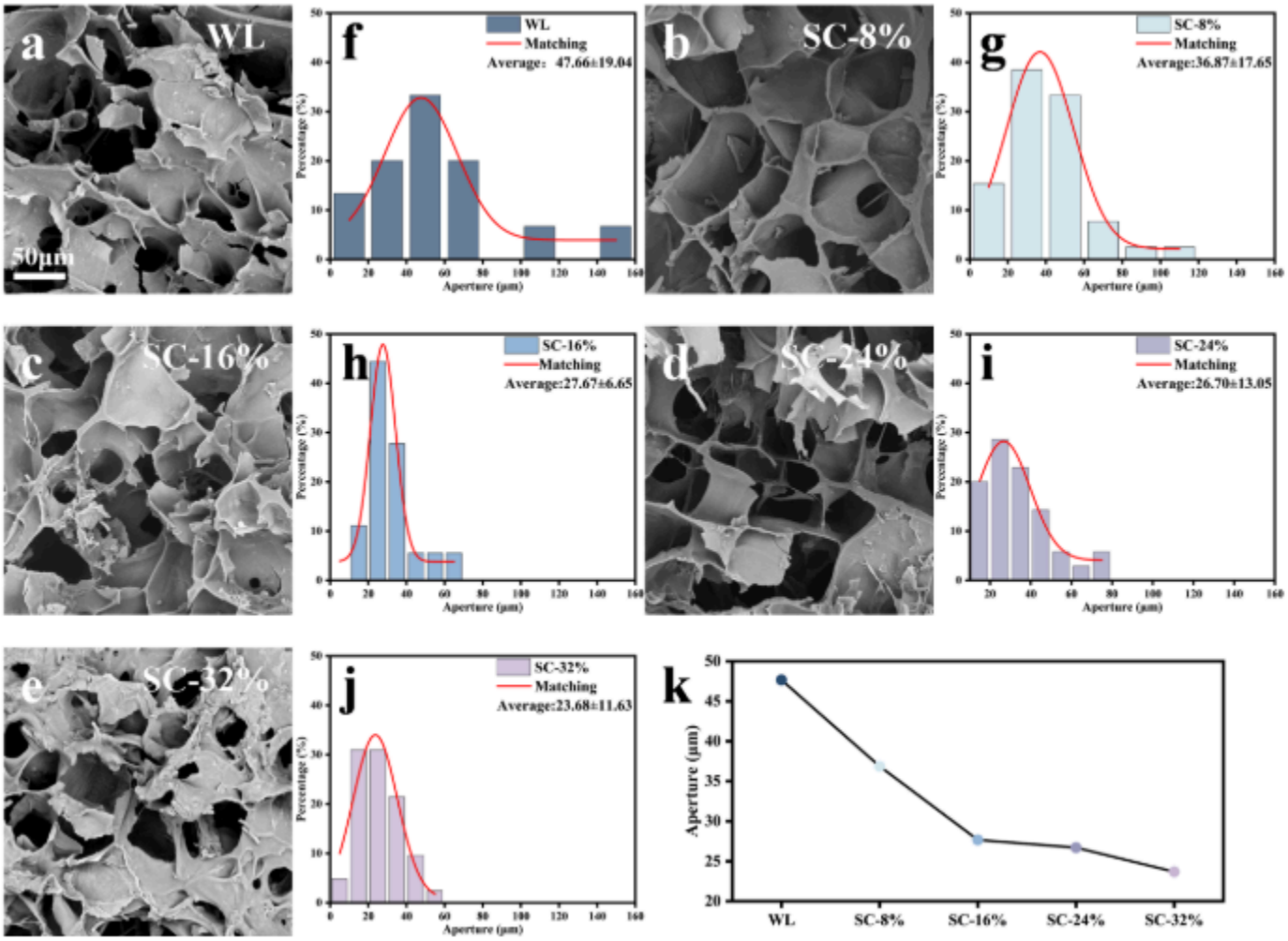


Figure 6

SEM analysis of SC-WLG: (a-e) Micrographs at 1000× magnification; (f-j) pore-size distributions; (k) Quantitative comparison of average pore size across formulations.

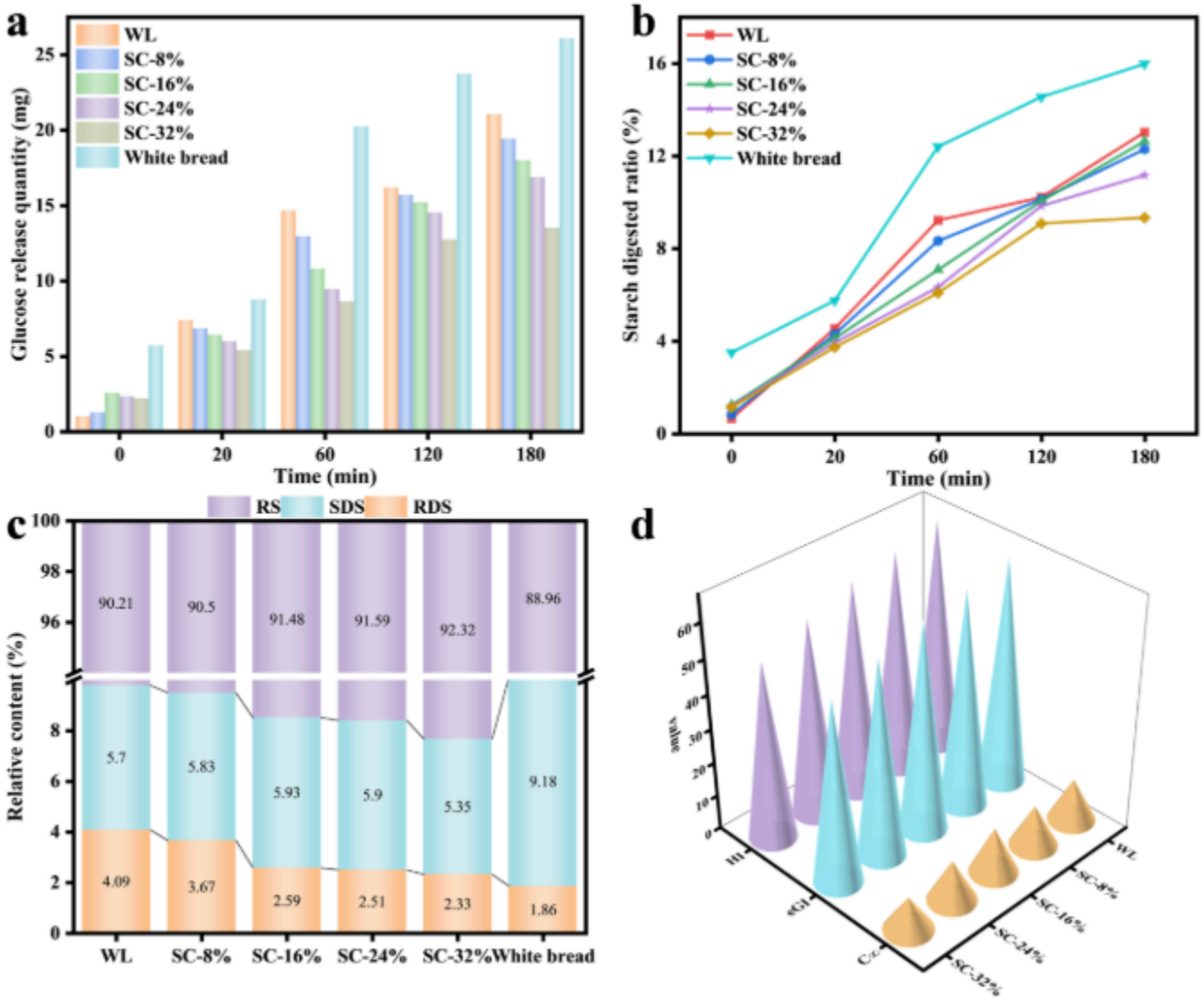


Figure 7

In vitro starch digestive properties of SC-WLG: (a) Glucose release; (b) Starch hydrolysis rate; (c) Starch composition. Including rapid digestible starch (RDS), slow digestible starch (SDS), and resistant starch (RS); (d) Hydrolysis index (HI), and estimated glycemic index (eGI) and maximum extent of hydrolysis (C∞).

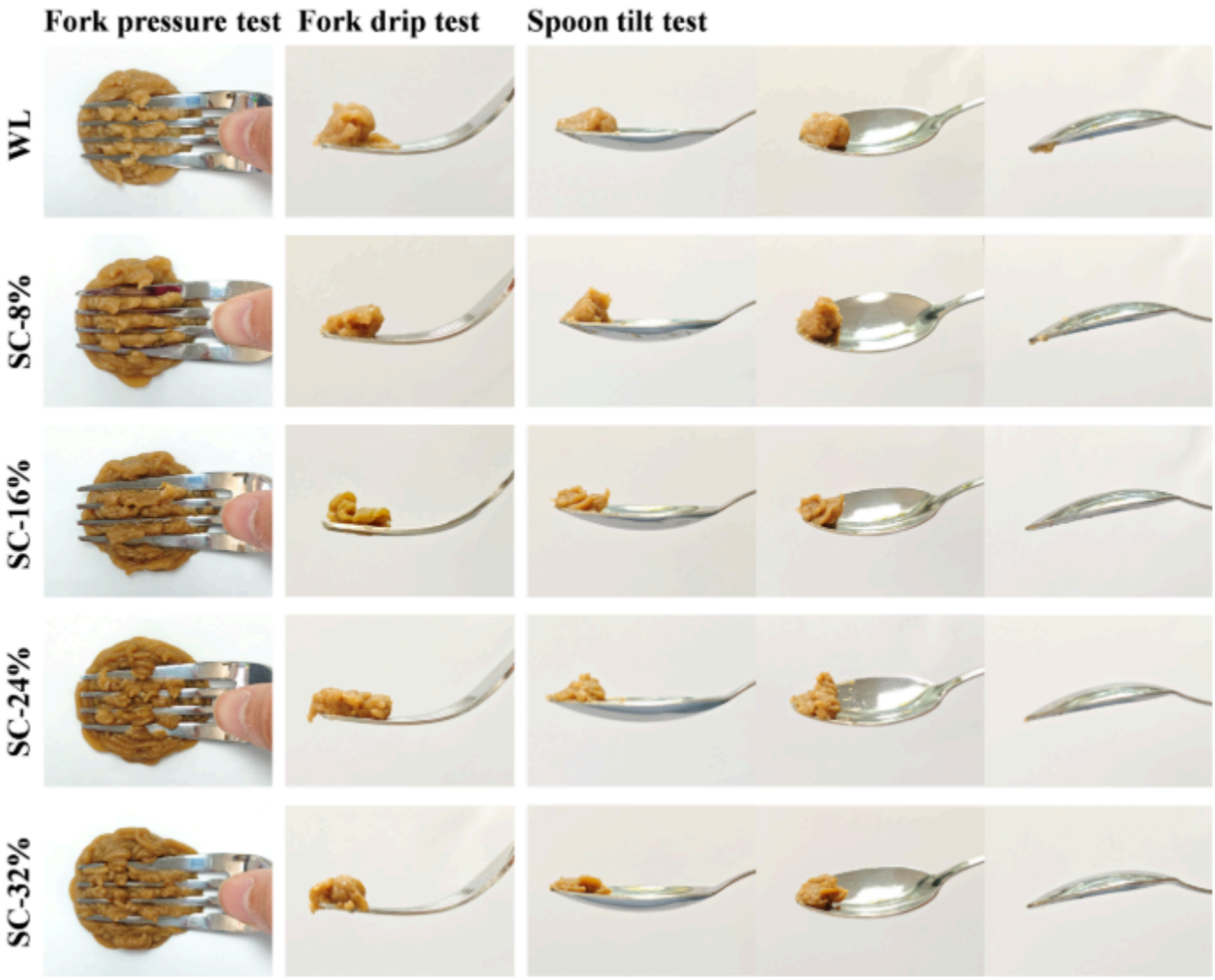


Figure 8

Qualitative IDDSI fork-pressure, fork-drip, and spoon-tilt assessments of SC-WLG.